

Stability of bubble-like fluxons in disk-shaped Josephson junctions in the presence of a coaxial dipole current

Cite as: Chaos **30**, 063132 (2020); <https://doi.org/10.1063/5.0006226>

Submitted: 28 February 2020 . Accepted: 02 June 2020 . Published Online: 16 June 2020

Alicia G. Castro-Montes, Juan F. Marín , Diego Teca-Wellmann, Jorge A. González, and Mónica A. García-Ñustes 

COLLECTIONS

 This paper was selected as Featured



View Online



Export Citation



CrossMark



NEW: TOPIC ALERTS

Explore the latest discoveries in your field of research

SIGN UP TODAY!



Stability of bubble-like fluxons in disk-shaped Josephson junctions in the presence of a coaxial dipole current

Cite as: Chaos 30, 063132 (2020); doi: 10.1063/5.0006226

Submitted: 28 February 2020 · Accepted: 2 June 2020 ·

Published Online: 16 June 2020



View Online



Export Citation



CrossMark

Alicia G. Castro-Montes,¹ Juan F. Marín,^{1,a),b)}  Diego Teca-Wellmann,² Jorge A. González,³ and
Mónica A. García-Ñustes¹ 

AFFILIATIONS

¹Instituto de Física, Pontificia Universidad Católica de Valparaíso, Casilla 4059, Chile

²Departamento de Física, Universidad Técnica Federico Santa María, Casilla 110-V, Valparaíso, Chile

³Department of Physics, Florida International University, Miami, Florida 33199, USA

^{a)}Author to whom correspondence should be addressed: juan.marin.m@usach.cl

^{b)}Present address: Departamento de Física, Universidad de Santiago de Chile, Av. Ecuador 3493, Estación Central, Santiago, Chile.

ABSTRACT

We investigate analytically and numerically the stability of bubble-like fluxons in disk-shaped heterogeneous Josephson junctions. Using ring solitons as a model of bubble fluxons in the two-dimensional sine-Gordon equation, we show that the insertion of coaxial dipole currents prevents their collapse. We characterize the onset of instability by introducing a single parameter that couples the radius of the bubble fluxon with the properties of the injected current. For different combinations of parameters, we report the formation of stable oscillating bubbles, the emergence of internal modes, and bubble breakup due to internal mode instability. We show that the critical germ depends on the ratio between its radius and the steepness of the wall separating the different phases in the system. If the steepness of the wall is increased (decreased), the critical radius decreases (increases). Our theoretical findings are in good agreement with numerical simulations.

Published under license by AIP Publishing. <https://doi.org/10.1063/5.0006226>

The controlled insertion, transport, and stability of fluxons in Josephson junctions (JJs) is a relevant problem for quantum information technologies. Of the various qubits that have been implemented, fluxon qubits are of particular interest because of their potential suitability for scalability and integration in superconducting circuits. In this work, we demonstrate how to stabilize and introduce bubble fluxons in Josephson junctions using a coaxial dipole current. Although point-like heterogeneities have been theoretically studied in similar one-dimensional systems, localized but not point-like heterogeneities have not been addressed analytically in two-dimensional junctions. We predict the formation of new oscillating states, generation of internal mode oscillations, expanding bubbles, and the breaking and insertion of new bubbles in the junction. Our results suggest a promising way for the storage and transport of information in quantum information devices.

I. INTRODUCTION

In the last three decades, a vast research area has been developed around the sine-Gordon (sG) system due to its many physical realizations.¹ The most significant ones are the fluxon dynamics in Josephson junctions (JJs),^{2–5} spin waves in magnetic materials,^{6,7} self-induced transparency in nonlinear optics,^{8,9} and the Frenkel–Kontorova model of dislocations in solid state physics.^{10–12} These applications are of great importance for both fundamental and technological motivations. A flux quantum in a JJ can be controlled by bias currents,³ created or perturbed by the insertion of dipole currents,^{13–15} pinned by built-in heterogeneities,^{16–18} or manipulated through shape engineering.^{4,19–21} Recent advances in the design of wave parametric amplifiers,^{22,23} quantum information processing protocols,^{23–26} and the controlled manipulation of heat currents in superconducting devices^{27–30} are promising applications of this system.

A fluxon in a JJ is a physical realization of a sG soliton.^{1,31} When a localized external dipole current perturbs a fluxon, the internal modes of the fluxon can be locally destabilized to produce the insertion of a local fluxon-antifluxon pair. This phenomenon is well understood in one-dimensional sG systems.^{32,33} In the two-dimensional case, the authors have recently reported the formation of a flux line closed in a loop with a radially symmetric bubble-like structure: a bubble fluxon.³⁴ The dynamics and stability of topologically equivalent structures in Klein–Gordon (KG) systems have gained significant attention in the literature, ranging from condensed matter to cosmology.^{4,35–43} Thus, theoretical studies on the formation, stability, and dynamics of bubble-like structures are relevant not only for heterogeneous sG systems but also for more general systems.

In this article, we give an analytical and numerical study of the stability of these bubble-like structures by the application of external forces. We demonstrate that the insertion of coaxial dipole currents may stabilize such structures. We provide a theoretical description of the response of bubble fluxons to the coaxial dipole current intensity, finding a stabilization domain. Furthermore, we show that internal mode dynamics generates remarkable phenomena, such as the formation of oscillating states, bubble instability, and bubble breakup. The article is organized as follows. In Sec. II, we present the system and the model of bubble fluxons in JJs. In Sec. III, we show analytically and numerically that the insertion of coaxial dipole currents in the junction stabilizes bubble fluxons. In Sec. IV, we perform the linear stability analysis of the bubble solutions. Finally, we give our conclusions and final remarks in Sec. V.

II. FLUXON BUBBLES IN JOSEPHSON JUNCTIONS

JJs are built as two superconductors separated by a thin dielectric layer.⁴⁴ A superconducting Josephson current composed by tunneling Cooper pairs crosses the junction. This produces a jump on the phase ϕ of the wave function of the superconducting electrons across the JJ. Such a tunneling current may create a loop that continuously goes from one superconductor to the other, forming the so-called Josephson vortex. These loops of current are represented by the well-known sG kink and antikink solutions, corresponding to a 2π -twist of superconducting phase ϕ .^{31,44} A Josephson vortex induces a local magnetic flux trapped in a JJ. Each sG kink carries a quantum of magnetic flux $\Phi_0 := h/2e$, where h is the Planck's constant. This is the so-called fluxon. Kink solutions are associated with fluxons, whereas antikink solutions are associated with antifluxons. Each direction of the loop of current is associated with the opposite signs of $\sin \phi(x)$ in different portions of the kink/antikink. Therefore, the center of the kink/antikink corresponds to the position of the fluxon/antifluxon.

The propagation of fluxons in disk-shaped JJs is governed by the following two-dimensional sG equation:^{31,44}

$$\partial_t \phi - \nabla^2 \phi + \gamma \partial_t \phi + \sin \phi = F(\mathbf{r}), \quad (1)$$

where $\phi = \phi(\mathbf{r}, t)$ is the quantum mechanical phase difference of the superconductors, $\mathbf{r} = (r, \theta)$ is the vector position in polar coordinates, and $\nabla^2 := \partial_{rr} + r^{-1} \partial_r + r^{-2} \partial_{\theta\theta}$ is the Laplace operator. The third term of the left-hand side of Eq. (1), which plays the role of dissipation, represents the normal component of the tunnel

current.⁴⁵ The space-dependent force $F(\mathbf{r})$ represents non-uniform external perturbations introduced in the junction, such as dipole devices of electrical current.^{14,15,46} Indeed, current dipole devices define an influx and an outflux zone separated by a small distance, creating a loop of electrical current in the junction. This loop of current induces a magnetic flux that perturbs nearby fluxons.

We investigate the stability of bubbles in JJs in the framework of the qualitative theory of nonlinear dynamical systems.⁴⁷ Bubbles of one phase in a space filled with another phase are heteroclinic trajectories joining fixed points of the underlying sG potential.⁴⁸ The coexistence of two heteroclinic solutions, one joining phases from ϕ_0 to ϕ_1 and other joining phases from ϕ_1 back to ϕ_0 , gives a model for a bubble profile. For instance, ring solitons,⁴⁹ kink–antikink pairs, and other topologically equivalent solutions are physically relevant models for bubbles.⁵⁰ Inspired on fluxon bubbles reported in two-dimensional JJs,^{34,37,51,52} we construct bubble-like profiles in the following manner. Circular ring soliton solutions of Eq. (1) are given by $\phi_R(r) = 4 \arctan \exp[-(r - r_0)]$, where r_0 denotes the radius of the soliton.^{49,51,52} In the case of a long one-dimensional JJ, it is known that a current dipole device may perturb the shape and the width of a fluxon^{32,33,50} (see Fig. 1). A local region of outflux (influx) current exerts a positive (negative) force in the 2π -wing (0-wing) of the fluxon. The soliton is being stretched due to these forces acting on its wings in opposite directions, changing its width.

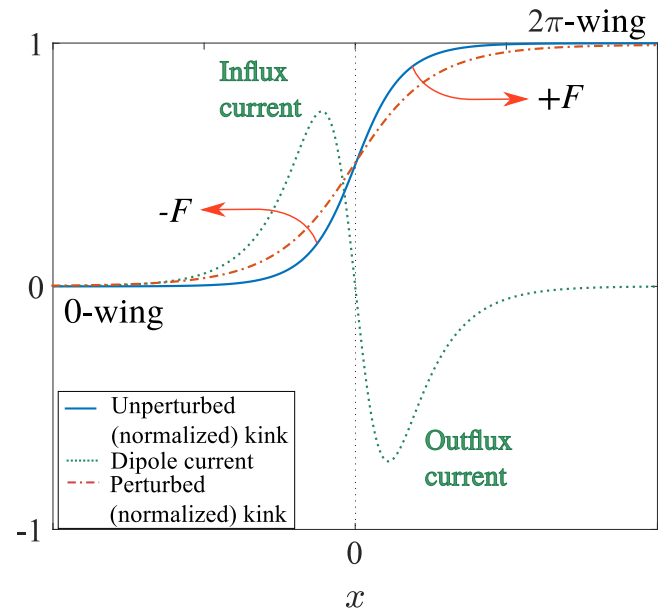


FIG. 1. Dynamics of a fluxon under the influence of a current dipole device in a long (one-dimensional) Josephson junction. The kink profile of the fluxon (normalized by 2π) is depicted in (blue) solid line. Under the influence of the current dipole, depicted in (green) dashed line, the fluxon is perturbed by counter-directed forces on its wings, producing a change on its width. The perturbed fluxon profile (normalized by 2π) is depicted in (red) dashed-dotted line.

The perturbed kink in its steady state is less steep than the unperturbed kink due to such a stretching, as depicted in Fig. 1. For sufficiently large values of the influx/outflux current, the fluxon can be destroyed by the stretching. This is associated with an internal (shape) mode instability, a phenomenon where the kink profile is no longer stable.^{32,33}

In the two-dimensional case, two-dimensional dipole currents may produce similar effects in the walls of a ring soliton. To take into account the change in the width of the wall of a ring soliton under the influence of some external force, we introduce a shape parameter B according to $\phi_R(r; B) = 4 \arctan \exp[-B(r - r_o)]$. Moreover, bubble-like fluxons must have a kink/antikink profile at the walls and a well-defined derivative in the limit $r_o \rightarrow 0$.³⁴ To obtain bubble-like profiles satisfying such conditions, we define the positive and negative bubbles as $\phi_+ := \phi_n - \phi_p$ and $\phi_- := \phi_p - \phi_n$, respectively, where $\phi_p(r) := 4 \arctan \exp[B(r - r_o)]$ and $\phi_n(r) := 4 \arctan \exp[B(r + r_o)]$. In Figs. 2(a) and 2(b), we depict these profiles, which have a bubble-like shape indeed. It follows that the bubble profile ϕ_{\pm} can be written in a more compact form as

$$\phi_{\pm}(\mathbf{r}) = 4 \arctan[\pm A \operatorname{sech}(Br)], \quad (2)$$

where $A := \sinh(Br_o)$ is a single real parameter that couples the two relevant parameters of our system, namely, B and r_o . Under no external perturbations, the bubble structure ϕ_{\pm} collapses toward its center where finally annihilates.^{37,51}

Knowing the behavior of heteroclinic solutions in the neighborhood of fixed points and separatrices, it is possible to construct other functions with the same topological properties. Thus, in the sense of the qualitative theory of nonlinear dynamical systems,⁴⁷ it is possible to generalize analytical results obtained for the solution of Eq. (2) to other bubble solutions that are topologically equivalent.

III. CONTROLLING BUBBLES WITH EXTERNAL PERTURBATIONS

For quantum information technologies, it is of crucial importance the control, the insertion, stability, and transport of fluxons. Thus, a natural question is whether we can control the bubble structures of Sec. II by the application of some external perturbation. Indeed, we have obtained that the insertion of a coaxial current dipole device in the junction can stabilize such structures.

Let us briefly consider Eq. (1) under a homogeneous and constant external force $F(\mathbf{r}) = f$. Stable solutions obey $\nabla^2 \phi - dU_{\text{eff}}(\phi)/d\phi = 0$, where $U_{\text{eff}}(\phi) := U(\phi) - f\phi$ is the effective potential, and $U(\phi) := 1 - \cos \phi$ is the sG potential. Stable and homogeneous solutions of such a system correspond to the minima of $U_{\text{eff}}(\phi)$ and describe different phases. Static bubbles represent configurations, where ϕ is in one phase everywhere except for a finite domain where it is in another phase. If $f = 0$, the potential $U_{\text{eff}}(\phi) = U(\phi)$ has infinitely many degenerate phases, and bubbles like Eq. (2) shrink. However, if $0 < |f| < 1$, $U_{\text{eff}}(\phi)$ has infinitely many barriers separating coexisting metastable phases. In this case, stationary bubbles in the sG system are similar to the nontopological solitons arising in nonlinear Schrödinger (NLS) systems with competing interactions,⁵³ which are well known to be unstable if they are not propagating.^{53,54} These non-propagating NLS-bubbles grow, converting a metastable phase to a more stable phase, thus seeding phase transitions.

Now let us return to the case of bubbles on Eq. (1) driven by a space-dependent force $F(\mathbf{r})$. Following the previous discussion, we notice that regions with $0 < |F(\mathbf{r})| < 1$ will introduce local competing interactions that may enhance the growth of non-propagating bubbles, whereas regions with $F(\mathbf{r}) = 0$ will enhance their collapse. Thus, a heterogeneous force may introduce the required balance to stabilize bubble-like structures such as Eq. (2). In the context of fluxon dynamics in JJs, the influence of a current dipole device is

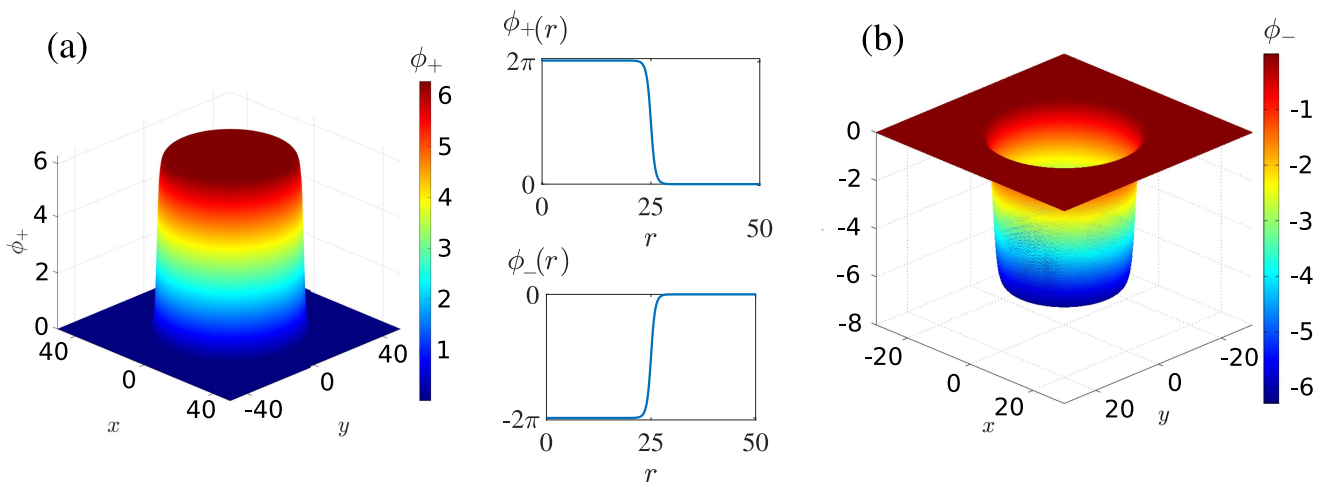


FIG. 2. (a) Positive and (b) negative bubble-like fluxons. The insets show the profile of each structure as a function of the radial coordinate r .

modeled through an additive space-dependent external force in the sG equation.^{13,14} Thus, to calculate the family of forces that can stabilize these bubble fluxons, we solve an inverse problem similarly to previous works.^{32,33,50,55} Let us consider the bubble profile of Eq. (2) as the initial condition. After substitution in the sG equation (1), we obtain that ϕ_{\pm} is an exact solution if the external force is given by

$$F_{\pm}(\mathbf{r}) = \left[\pm 2(B^2 - 1)\alpha(r) + \frac{2B}{r}\beta(r)\tanh(Br) + \Upsilon(\alpha(r) - \beta(r)) \right] \operatorname{sech}(Br), \quad (3)$$

$$\alpha(r) := -2A \frac{1 - A^2 \operatorname{sech}^2(Br)}{[1 + A^2 \operatorname{sech}^2(Br)]^2}, \quad \beta(r) := \frac{-2A}{1 + A^2 \operatorname{sech}^2(Br)}, \quad (4)$$

where $\Upsilon := 2B^2/A^2$. Figure 3 shows F_+ for the given values of parameters. It is important to remark that as $r \rightarrow 0$, the second term in the square brackets of Eq. (3) goes to zero since the factor $\beta(r)\tanh(Br)$ decays to zero exponentially in that limit. Regions with $F_{\pm} < 0$ ($F_{\pm} > 0$) correspond to an area in the junction with an influx (outflux) of current. A coaxial dipole current is defined by an influx and outflux zone separated a distance D . Given the current distributions, such zones have a finite decay width. This latter is physically consistent with an actual dipole current in experimental setups, where point-like dipoles are not realistic. If the distance D is of the order of the decay width, the dipole is no longer defined. The dipole existence range is determined by the interplay of both B and r_0 . In Fig. 3(b), we show that F_+ represents a coaxial dipole current for $r_0 = 25.0$, $B = 1.2$, and $B = 0.8$. For $B = 1$, the distance D is smaller than the decay width and, therefore, the force F_+ cannot be regarded as a dipole current. If the force has a dipole profile,

such a pair of influx/outflux current generates a local magnetic field that affects the dynamics of fluxons in the junction. Indeed, from a purely geometrical point of view, this ring-like force can be regarded as a solid of revolution formed by the dipole currents considered in Refs. 13, 14, and 34. The total current $I \propto \int dV F_{\pm}(r)$ from the dipole is always negative. Therefore, the dipole is injecting current into the junction, providing energy that can be used to stabilize fluxon bubbles. The axial symmetry of the force allows the manipulation of rotationally symmetric localized structures, such as bubbles. Notice that parameter B is associated with both the intensity of the current and the spatial extension of the injection area.

We have performed numerical simulations of Eq. (1) with the positive bubble ϕ_+ from Eq. (2) as the initial condition, homogeneous Neuman boundary conditions, and $\gamma = 0.01$. For the Laplace operator, we have used finite differences of second-order accuracy with steps $dx = dy = 0.1$. The time integration was performed using a fourth-order Runge-Kutta scheme. Figure 4 shows the result for the given values of the parameters. Figure 4(a) shows a positive bubble perfectly stabilized by F_+ . This is the equilibrium configuration of the system, where both the bubble and the force has the same radius (see inset with the profiles of ϕ_+ and F_+ at $y = 0$). Moreover, we can also consider coaxial forces with a different radius than the initial bubble. Numerical simulations show that for $B = 1.2$, the force stabilizes bubbles if the difference between the radii is at most 10% of the bigger radius. That is, if the initial radius of the bubble is smaller by more than a 10% of the radius of the force, then the coaxial dipole current is too far from the walls of the bubble to prevent its collapse. The bubble collapses almost as it were unperturbed. If, on the other hand, the initial radius of the bubble is bigger by more than a 10% of the radius of the force, then the bubble begins to shrink for enough time to gain relatively high speed. The coaxial dipole cannot capture the wall of the bubble because it passes very fast, and the bubble collapses.

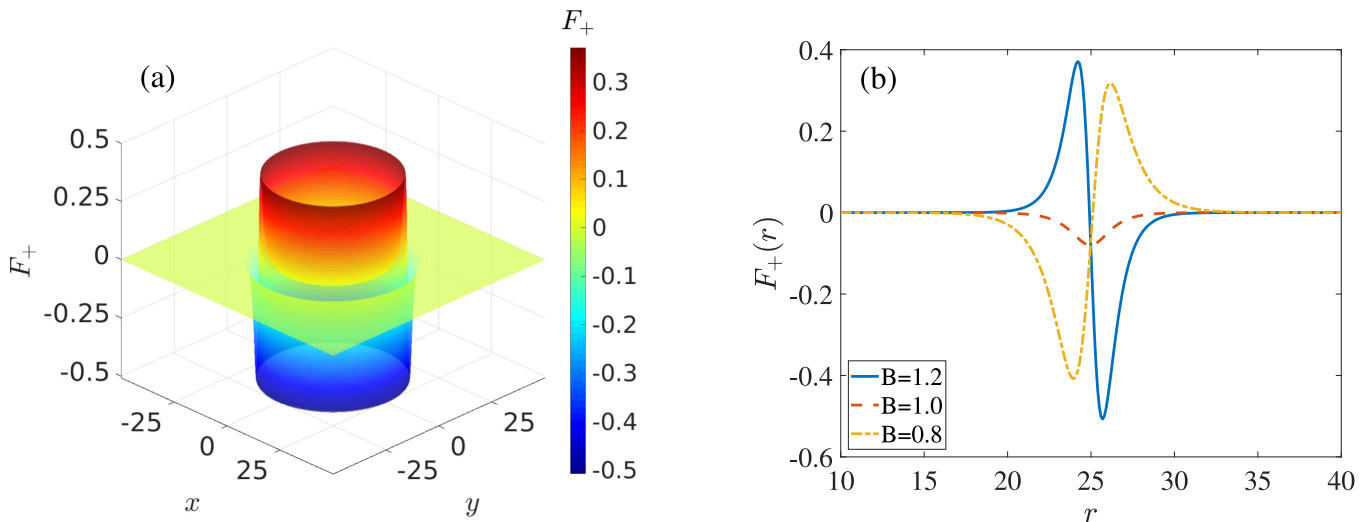


FIG. 3. (a) The ringlike force of Eq. (3) for $B = 1.2$, modeling a coaxial current dipole with a radius $r_0 = 25.0$ inserted into the Josephson junction. (b) Profile of F_+ as a function of r for $r_0 = 25.0$ and different values of B .

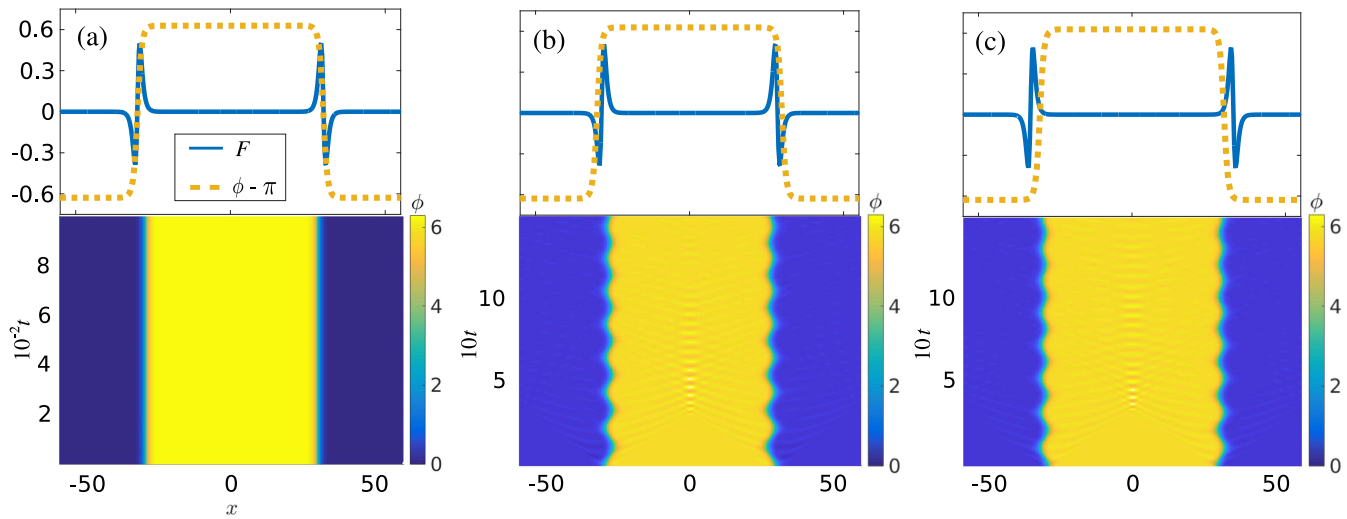


FIG. 4. Spatiotemporal evolution of bubble fluxons with an initial radius r_0 under the action of a coaxial dipole current with a radius R for $\gamma = 0.01$, $B = 1.2$, and $dt = 0.005$. (a) A stable positive bubble for $r_0 = R = 30.0$. (b) An oscillating state for $r_0 = 30 > R = 28.5$. The area of the bubble performs damped oscillations around the equilibrium radius R . (c) An oscillating state for $r_0 = 30.0 < R = 31.5$. The upper insets show the profile at $y = 0$ of the initial bubble and the ring-like force for each case.

In any other circumstance, the wall of the bubble does not have enough time to gain too much speed, and the coaxial dipole traps the bubble, preventing its collapse. In Fig. 4(b), we show the formation of an oscillating bubble solution for the given values of the parameters. The initial condition is a fluxon bubble whose radius is bigger than the radius of the force. The bubble shrinks and is captured by the dipole, making damped oscillations in time around the equilibrium configuration. In Fig. 4(c), we show the formation of a similar oscillating state from a bubble whose radius is smaller than the radius of the force. In this case, the bubble is expanded due to an attractive interaction with the coaxial dipole, making again damped oscillations around the equilibrium configuration.

IV. STABILITY ANALYSIS OF BUBBLE FLUXONS

In this section, we perform a linear stability analysis of the bubble solutions of Eq. (2) under the action of the ring-like force of Eq. (3). For that purpose, we write the perturbed sG equation (1) as

$$\partial_t \phi - \nabla^2 \phi + \gamma \partial_t \phi - G(\phi) = F(\mathbf{r}), \tag{5}$$

where $G(\phi) := -dU/d\phi$ and $U(\phi) := 1 - \cos \phi$. To investigate the stability of the structure ϕ_{\pm} , let us consider a small-amplitude perturbation χ around such solution, i.e.,

$$\phi(\mathbf{r}, t) = \phi_{\pm}(\mathbf{r}) + \chi(\mathbf{r}, t), \tag{6}$$

$$\chi(\mathbf{r}, t) := f(\mathbf{r})e^{\lambda t}, \quad |\chi| \ll |\phi_{\pm}| \forall (\mathbf{r}, t), \tag{7}$$

with $\lambda \in \mathbb{C}$. Expanding $G(\phi)$ with $\phi \sim \phi_{\pm}$ neglecting terms of order $\mathcal{O}(|\chi|^2)$, and after substitution of Eqs. (6) and (7) in the sG equation (1) with $F(\mathbf{r}) = F_{\pm}(\mathbf{r})$, we obtain for $f(\mathbf{r})$ the following

eigenvalue problem:

$$-\nabla^2 f + V_{\pm}(r)f = \Gamma f, \tag{8}$$

with

$$\Gamma := -\lambda(\lambda + \gamma), \tag{9}$$

where $V_{\pm}(r) := \cos \phi_{\pm}(r) - 1$. Equation (8) is equivalent to the time-independent Schrödinger equation. The potential $V_{\pm}(r) := 1 + V(r)$ is the same for both structures, the positive and negative bubbles, where $V(r)$ is given by

$$V(r) = -\frac{8A^2 \operatorname{sech}^2(Br)}{[1 + A^2 \operatorname{sech}^2(Br)]^2}. \tag{10}$$

From potential (10), we can identify two delimited regions of parameter A for which the system exhibits different qualitative behaviors. Figure 5(a) shows the profile at $y = 0$ of the potential (10) for different values of A . For $A \leq 1$, Eq. (10) at $y = 0$ is a hyperbolic potential well, while for $A > 1$, it is a hyperbolic double-well potential, as shown in Fig. 5(a). Indeed, for $A < 1$, the potential (10) has only one real and stable equilibrium point at the origin. Above the critical value $A = A_c := 1$, the equilibrium point at the origin turns unstable, and two new real stable points appears at $x = x_{\pm} := \pm B^{-1} \operatorname{acosh}(A)$. Thus, at $A = A_c$, the profile of potential V passes from a single-well to a double-well structure through a pitchfork bifurcation, as shown in Fig. 5(b). The system has very different dynamics in each region, which are separated by the bifurcation point $A = A_c$. In the following, we investigate the dynamics of the system in each region.

A. The double-well region ($A > 1$): Stable bubbles, oscillating states, generation of internal modes, and bubble insertion

In the case $A > 1$, the potential of Eq. (10) has a double-well structure, as depicted in Fig. 6 for different values of B . We notice that if $A \rightarrow \infty$, then $V(0) \rightarrow 0$ and $x_{\pm} \rightarrow \infty$, which means that the separation of the minima of the double-well increases indefinitely as $A \rightarrow \infty$. This behavior can also be seen in Fig. 5(a). Therefore, in the limiting case $A \gg 1$, the double-well potential (10) can be regarded as two independent single wells very far from each other. Let us define $\xi := \text{sech}(Br)$ and $\xi_{\pm} := \text{sech}(Bx_{\pm})$. After a Taylor expansion of the potential with $\xi \sim \xi_{\pm}$, and noticing that $\xi_{\pm} \rightarrow 0$ as $A \rightarrow \infty$,

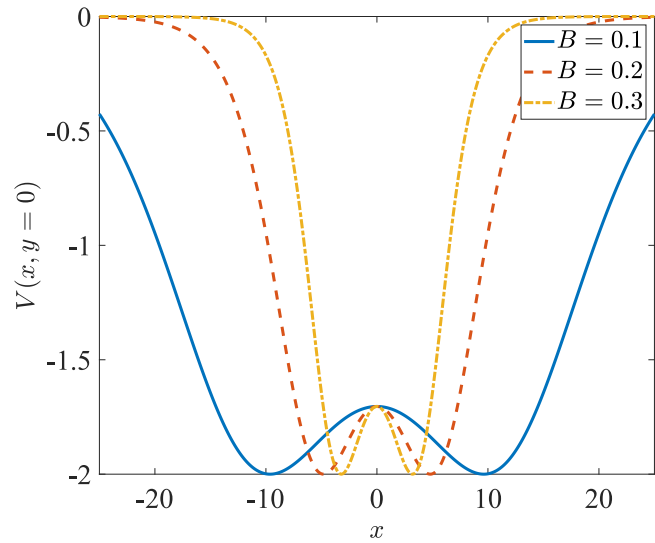


FIG. 6. The double-well potential of Eq. (10) at $y = 0$ for $A = 1.5$ and the given values of B . The walls of the double-well become steeper as B increases.

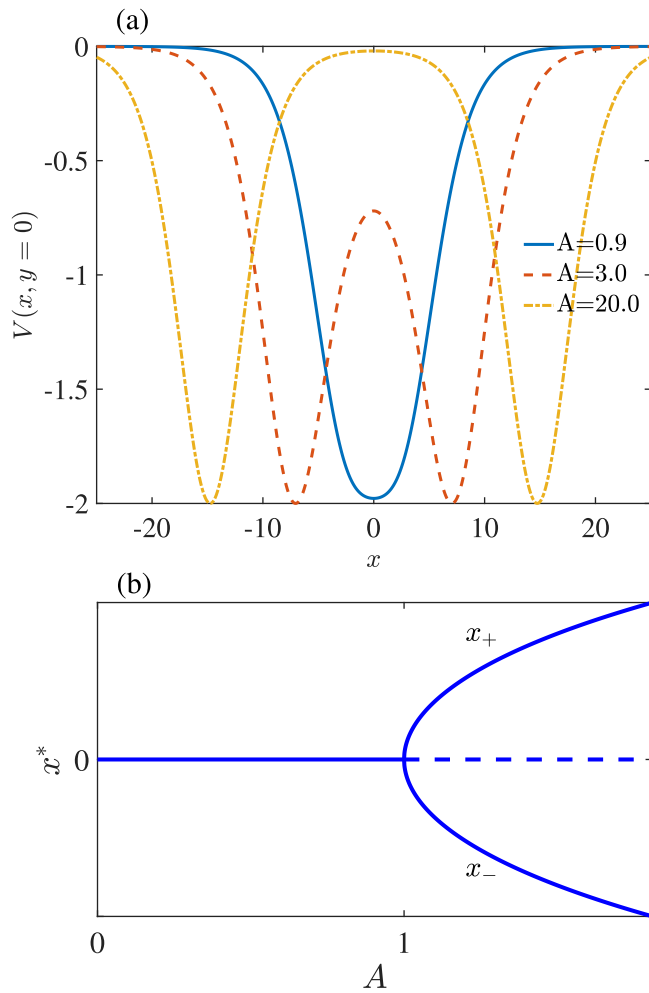


FIG. 5. (a) Potential of Eq. (10) for $B = 0.25$ and the indicated values of A . At $A = 1$, the system bifurcates from a single-well to a double-well potential. (b) Bifurcation diagram of $V(x, y = 0)$, showing the position of the equilibrium (fixed points) at the origin, x_+ and x_- as a function of the bifurcation parameter A . A pitchfork bifurcation occurs at $A = A_c = 1$. Solid lines denote stable fixed points, whereas dashed lines denote unstable fixed points.

one obtains that the potential behaves locally for $r \sim x_+$ as

$$V(r) \simeq -2 \text{sech}^2[B(r - x_+)], \tag{11}$$

which is the so-called modified Pöschl–Teller potential hole.⁵⁶ Thus, away from the bifurcation point, the double-well potential of Eq. (10) behaves as two effective Pöschl–Teller potentials far from each other.

Notice that from the condition $A \gg 1$ follows $Br_o \gg 1$, which means that the radius of the bubble is much greater than $1/B$. In such a limit, the curvature effects are negligible ($\nabla^2 \simeq \partial_{rr}$). Thus, the system can be regarded as quasi-one-dimensional, obtaining a good estimate of the bound states of the eigenvalue problem (8) by solving the Schrödinger equation at each well separately. Indeed, the Schrödinger equation (8) for the Pöschl–Teller potential can be solved exactly⁵⁶ and has appeared previously in the literature for the stability analysis of many nonlinear structures, such as one-dimensional sine-Gordon kinks.^{32,33,50,55,57} The eigenfunctions determine the oscillations around the bubble solution. The scattering states, corresponding to the continuous spectrum, are generally called phonon modes.⁵⁸ Meanwhile, the soliton modes correspond to the bound states, whose eigenvalues lay in the discrete spectrum⁵⁹ and are given by the formula

$$\Gamma_n = B^2(\Lambda + 2\Lambda n - n^2) - 1, \tag{12}$$

with $\Lambda(\Lambda + 1) = 2/B^2$. The integer part of Λ , $[\Lambda]$, yields the number of eigenvalues in the discrete spectrum ($n < [\Lambda]$), including the translational mode Γ_0 and the internal shape modes Γ_n with $n > 0$. Notice that for $B^2 = 1$ we obtain $\Gamma_0 = 0$, and the system possesses translational invariance for r sufficiently large. This zero-frequency bound state is the Goldstone mode.

We can now predict theoretically the response of fluxon bubbles to the coaxial dipole current for different values of the control

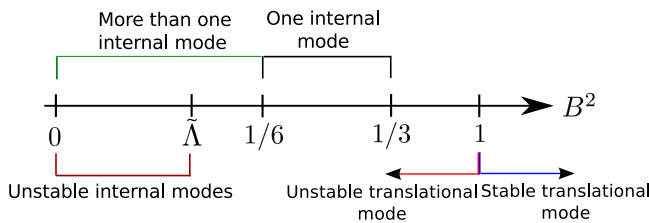


FIG. 7. Schematization of the results obtained from the linear stability analysis in the double-well region ($A \gg 1$).

parameter B . Figure 7 summarizes the results. Such results are valid for both positive and negative bubble solutions.

1. Stability of the translational mode

Returning to Eq. (9), we note that Γ has a quadratic dependence on λ with roots $\{0, -\gamma\}$ and a maximum $\Gamma_{\max} = \gamma^2/4$ at $\lambda_{\max} = -\gamma/2$. From Eq. (9) follows $\lambda = (-\gamma \pm \sqrt{\gamma^2 - 4\Gamma})/2$, which can be complex if γ is small. Near the origin ($\lambda = 0$), the stability of the mode is determined by the sign of Γ , being stable (unstable) if $\Gamma > 0$ ($\Gamma < 0$). Thus, if the n th mode is stable ($\Gamma_n > 0$) and $\gamma^2 - 4\Gamma < 0$, the bubble walls will oscillate at a frequency $\omega_n = \sqrt{4\Gamma_n - \gamma^2}/2$ with a decay rate of $-\gamma/2$. On the contrary, if the n th mode is unstable ($\Gamma_n < 0$), the mode grows with no oscillations.

Imposing $\Gamma_n > 0$, we obtain the conditions for stability of the n th mode in terms of the control parameter B^2 . Thus, the condition for stability of the translational mode ($\lambda_0 < 0$) is $B^2 > 1$.^{32,33,50} In this case, the ring-like force stabilizes the bubble to a fixed radius equal to the radius of the force itself. Indeed, the combination of parameters of the numerical simulations showed in Fig. 4 corresponds to this case, and the theory predicts the stability of the bubble correctly. In the simulation of Fig. 4(a), the core of the bubble wall is exactly at the stable equilibrium position, and the bubble is completely stationary. If we displace the core of the wall from this equilibrium point slightly, then the wall oscillates around the stable equilibrium—see Figs. 4(b) and 4(c). We calculate the frequency of oscillation of

such states computing the fast Fourier transform of the bubble-wall position in time. For the states shown in Figs. 4(b) and 4(c), we obtain $\omega = 0.29$ ($T = 21.9443$) and $\omega = 0.33$ ($T = 19.2012$), respectively. These values are in great agreement with the theoretical translational-mode frequency ω_0 for $B = 1.2$.

If $1/3 < B^2 < 1$, the translational mode becomes unstable with no oscillations and no internal modes.^{32,33,50} Under these conditions, the equilibrium points x_{\pm} are now unstable. Therefore, if the initial radius of the bubble is smaller than the radius of the ring-like force, the bubble will collapse. If on the contrary, the initial radius of the bubble is bigger than the radius of the force, the external force will push the bubble wall away, and the bubble will expand. Eventually, the curvature force that tends to collapse the bubble compensates the repulsion due to the ring-like force. The acceleration of the bubble expansion will be zero when one force equilibrates the other, and eventually, the bubble wall will go backward.

The dynamical behavior observed in Fig. 8(a) agrees with these theoretical findings. The initial condition is a positive bubble, which has a radius r_0 slightly bigger than the radius r_f of the coaxial dipole current. The instability of the translational mode produces a motion of the bubble wall away from the unstable fixed point located at the zero of the force. This instability along with the return effect produces the oscillatory behavior of the bubble area, as expected. Note that the origin of these oscillations is different than those observed in Figs. 4(b) and 4(c).

2. The existence of stable internal modes

The repulsion from the dipole current becomes stronger, and the translational mode turns more unstable as B decreases. Indeed, we notice in the simulation of Fig. 8(b) that the bubble reaches a bigger radius during the first burst than in Fig. 8(a). The oscillating states of Fig. 4 are similar to the oscillating state of Fig. 8(a).

Although the dynamics of the bubble in Fig. 8(b) is similar as in Fig. 8(a), we notice the presence of small oscillations near the zero of the ring-like force in this last case. This is, indeed, evidence of the existence of a stable oscillatory-internal-mode in the system. Indeed, if $1/6 < B^2 < 1/3$, the translational mode is unstable and the first internal mode of the bubble will appear.^{32,33,50} In this case, we obtain

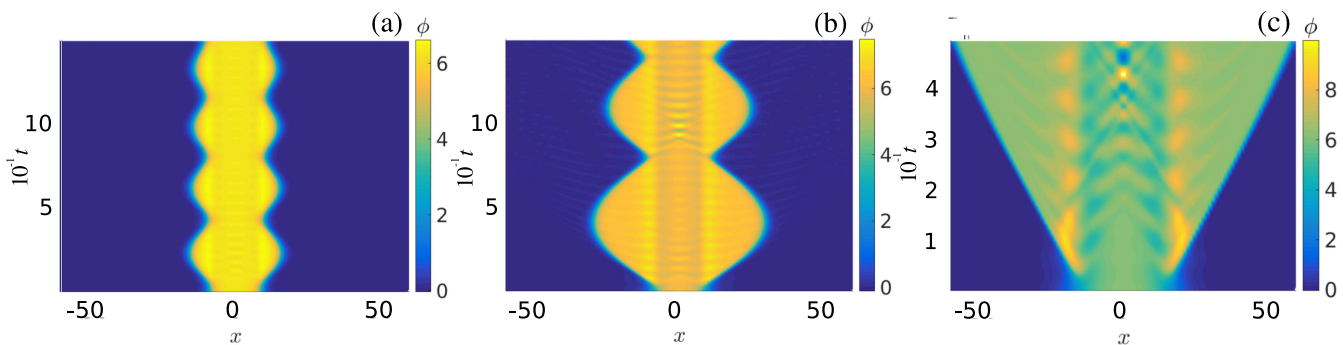


FIG. 8. (a) A stable bubble due to the equilibrium of competing forces for $(B, r_0, r_f) = (0.8, 8.7, 8.3)$. (b) A stable bubble oscillating at a lower frequency for $(B, r_0, r_f) = (0.5, 8.7, 8.3)$. The oscillations from a stable internal mode can be clearly appreciated. (c) An unstable bubble for $(B, r_0, r_f) = (0.261\ 50, 16, 15.3)$. The oscillations of the internal mode become more complex due to the emergence of more than one internal mode. In all cases, $dt = 0.05$.

$\lambda_1 < 0$. Therefore, this internal mode is stable. The width of the bubble walls will be oscillating at a frequency equal to $\omega_1 \approx \sqrt{\Gamma_1}$. The numerical simulation of Fig. 8(b) is in this range of parameters. Given that the translational mode of the wall is still unstable in this case, the bubble area initially expands. The parameter B is lower in this case than in the previous simulation. Thus, the maximum of the ring-like force is bigger and the bubble expands.

In case $B^2 < 1/6$, more internal modes will appear,^{32,33,50} and the oscillations in the walls become complex. There is a contribution of more than one frequency in this case. The simulation of Fig. 8(c) illustrates this scenario. More than one stable internal modes are present in the system, and the collapsing force is too weak compared to the repulsion from the current dipole. The translational mode is highly unstable, and the bubble expands.

3. Bubble breakup by internal mode instability

We have seen that for sufficiently small values of B , the translational mode of the bubble wall can become unstable. An important question is whether the internal modes of the wall can also become unstable for sufficiently small values of B . Indeed, if $B^2 < \tilde{\Lambda}$, where $\tilde{\Lambda} := 2/\Lambda^*(\Lambda^* + 1)$ and $\Lambda^* := (5 + \sqrt{17})/2$, the first internal mode becomes unstable.^{32,33,50} Figure 9 shows the bubble breakup. The initial bubble expands due to the instability of the translational mode, but soon after this expansion, more structures are inserted in the system by the coaxial dipole current. This insertion of new structures is due to the creation of a pair kink–antikink in the wall of the initial bubble.

Figure 9(a) shows that a new structure is inserted in the system around $t = 0.17$ for $B = 0.261$. The internal shape-mode instability produces the breaking of the wall of the bubble, and it acquires a ladder-like profile that expands in time. This new structure is a *disk-shaped bubble*, whose inner and outer radius is denoted as R_i and R_o , respectively. The inner (outer) wall of the inserted disk-shaped bubble is an antikink (kink) and, therefore, is trapped (ejected) by the coaxial force. Thus, R_i performs damping oscillations around the equilibrium point r_j while R_o grows in time, as we show in Fig. 9(a). The generated disk-shaped bubbles are always expanding structures.

The number of inserted bubbles depends on the actual value of parameter B . Figure 9(b) shows that more bubbles are rapidly inserted in the system for $B = 0.255$. The generated traveling ladder has more steps for decreasing values of parameter B . Figure 10 shows a typical configuration of the system after the initial breakup of the bubble, where an expanding disk-shaped bubble is appreciated.

B. The single well region ($A < 1$): Unstable bubbles

In the case $A < 1$, Eq. (10) for $y = 0$ is a potential well—as previously shown in Fig. 6. Moreover, in the limiting case $A \ll 1$, it reduces to

$$V(r) = -8A^2 \operatorname{sech}^2(Br), \tag{13}$$

which is also a Pöschl–Teller potential hole whose exact solutions are known.⁵⁶ However, here, we show that in this region of parameters, the force F_{\pm} is no longer a coaxial dipole, and the system does not support stable bubble solutions.

In sG systems, as in more general KG systems, it is well known that the zeroes of an external force are fixed points for kink and

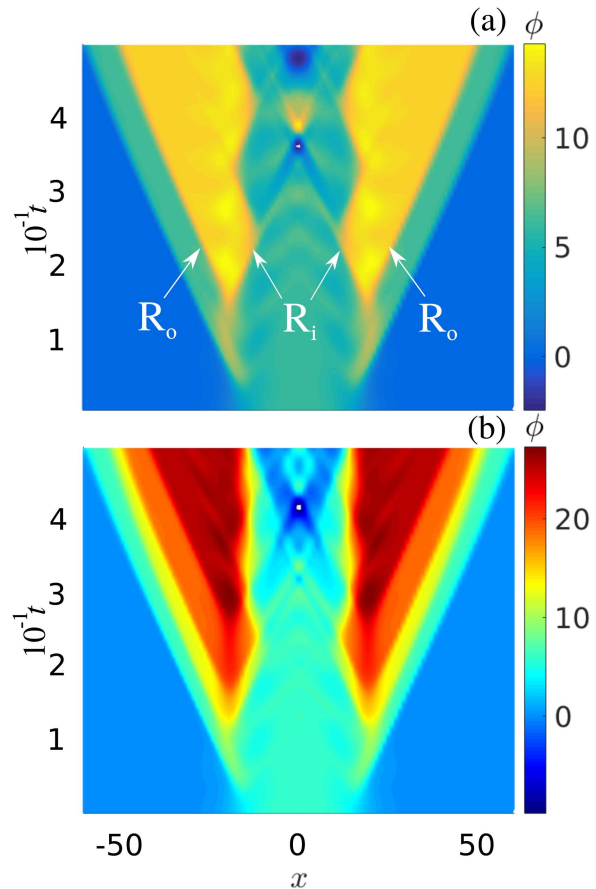


FIG. 9. Bubble breakup obtained with $dt = 0.05$ and (a) $B = 0.261$ and (b) $B = 0.255$. In both cases, $r_o = 16$ and $r_i = 15.3$.

antikink solutions.^{32,33} Given that the walls of the bubble solutions ϕ_{\pm} can be regarded as a pair kink–antikink in the r -domain, the zeroes of F_{\pm} are fixed points that may stabilize the structure. Figure 11 shows the force as a function of x at $y = 0$ for the given values of A . For $A > 1$, that is, in the double-well regime, the force has two fixed points that may contribute to the stabilization of bubble fluxons. If the fixed points are stable, a nearby bubble wall will be attracted by the fixed points, and either a stationary or an oscillatory bubble will be observed. This is the case of the simulations of Fig. 4. On the contrary, if the fixed points are unstable, then a nearby bubble wall will be ejected from the fixed point, and one would observe one of the structures reported in Figs. 8 and 9.

Diminishing the value of A toward $A_c := 1$, the system approaches the bifurcation point, and the zeroes of the force approach each other. This is indicated in Fig. 11 by the direction of the red arrows. The minima of the associated double-well potential have similar behavior as the fixed points of the walls as $A \rightarrow 1$. At the bifurcation point, the two fixed points collide and annihilate each other! At this point, the external force is no longer a coaxial dipole. For $A < 1$, there are no fixed points, and the system does not

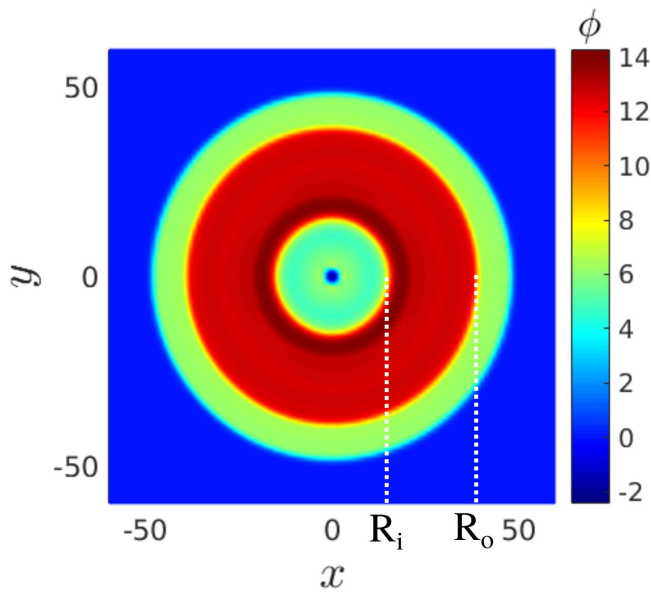


FIG. 10. An expanding $2\pi-4\pi$ disk-like bubble generated inside the initial $0-2\pi$ bubble for $B = 0.261$, $r_o = 16$, $r_i = 15.3$, and $t = 0.725$.

support stable bubble solutions anymore. Numerical simulations have confirmed our analysis. All bubbles in this region of parameters collapse.

Figure 12 shows a representation of the parameter space that summarizes our findings. The blue (red) region denotes

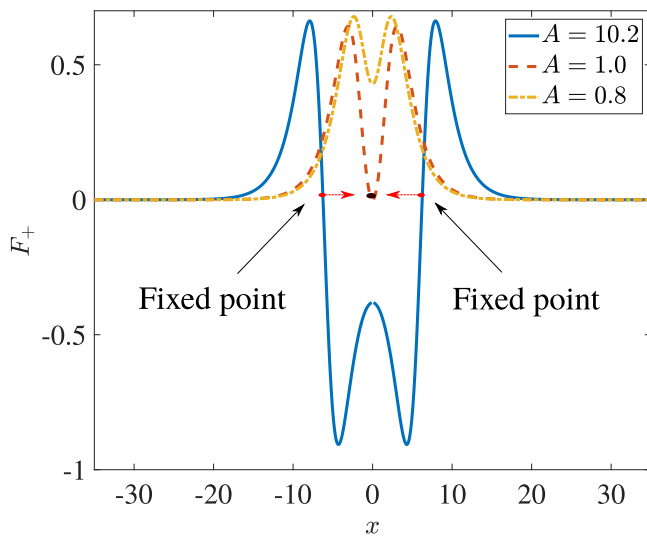


FIG. 11. Profiles of the coaxial force F_+ for $B = 0.5$, $y = 0$, and the indicated values of A as a function of x . For $A = 10.2 > 1$ ($r_o \simeq 6.0359$), the force has two fixed points for the position of the bubble walls. At $A = 1$ ($r_o \simeq 1.7627$), such stable points collide at the origin. For $A = 0.8 < 1$ ($r_o = 1.4653$), there are no fixed points, and the system does not support stable bubble solutions.

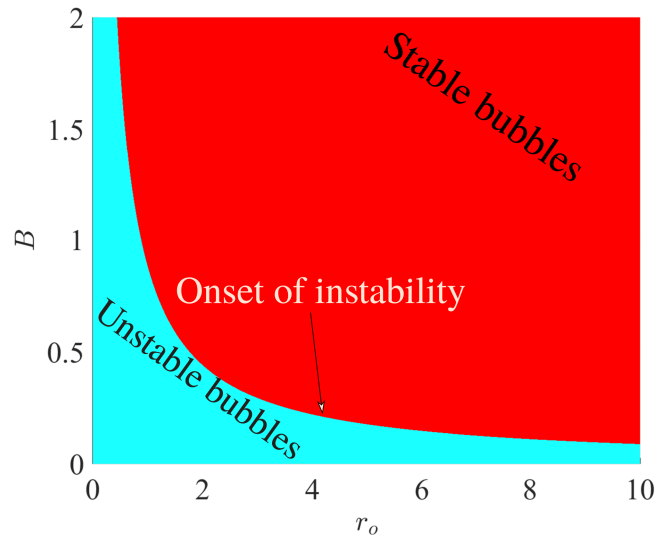


FIG. 12. Parameter space $\{r_o, B\}$, indicating the regions for stable and unstable bubble fluxons. The boundary between both regions is given by the points satisfying the condition $A_c = \sinh(Br_o)$, which gives the onset of instability.

combinations of parameters, where bubble fluxons are unstable (stable). Bubble fluxons are stable for $A > 1$ and unstable for $A < 1$. The onset of instability that determines the boundary between both regions is given by the condition $\sinh(Br_o) = 1 = A_c$. Thus, the stability of bubble fluxons is described by a single parameter A that couples the two relevant parameters of the system. Given that r_o is related to the equilibrium radius of the bubble fluxon and B is related to the injected current, from Fig. 12, it is possible to determine the coaxial dipole current needed for the stabilization of a bubble with a given radius.

The bubble fluxons studied in this work can be regarded as a structural phase transition, where the superconducting phase difference is driven to a new phase by an instability. In order to produce a transition from one phase to another, a critical germ (a bubble with a minimum critical radius) is usually considered in the literature for the development of an instability that is energetically above a nucleation barrier.^{50,60} In our model, the condition $r_o > 1/B$ holds for bubbles with steep walls, where the bubble decay length is smaller than its radius. This case corresponds to $A > 1$, which is above the onset of instability. Thus, a bubble fluxon can be stabilized by a coaxial dipole if the steep of the walls is large compared to its radius. Conversely, the region $A < 1$ corresponds to the condition $r_o < 1/B$, which holds when the bubble decay length is larger than its radius. In this case, the bubble is almost collapsed near the origin and there is no coaxial dipole capable of preventing its annihilation. Previous works have considered the critical germ only in terms of the minimum radius required in the field configuration $\phi(\mathbf{r}, t)$.^{50,60-63} The results from our model lead us to the important conclusion that the critical germ is determined by an interplay between its radius and the steepness of the wall separating the different phases in the system. If the steepness of the wall is increased (decreased), the critical radius decreases (increases).

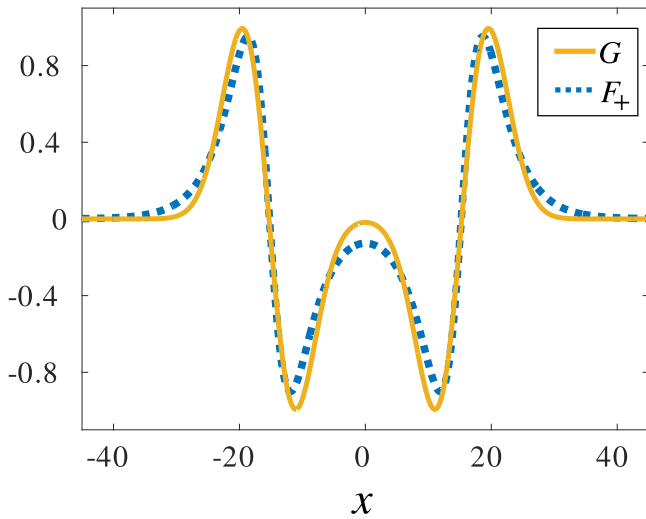


FIG. 13. Comparison of topologically equivalent forces for $\gamma = 0$. The external force of Eq. (3) is depicted in (blue) dashed line for $B = 0.261$ and $r_f = 15.3$. The equivalent force of Eq. (14) is depicted in (yellow) solid line for $\gamma = 3.2$, $\sigma = 4.2$, $r_o = 15.3$, and $a = 1.1$.

V. CONCLUSIONS AND FINAL REMARKS

We have investigated theoretically and numerically the stability of bubble-like fluxons in two-dimensional Josephson junctions. Although they are unstable under no external perturbations, we have shown that such structures can be stabilized by the insertion of coaxial current dipole devices. Using a single parameter $A := \sinh(Br_o)$ that couples the geometrical properties of the bubble and the coaxial dipole, we have determined the condition for the formation of stable bubbles. We have predicted theoretically the creation of oscillating states, the generation of internal mode oscillations and the bubble breakup due to shape mode instabilities. We have also obtained that the steepness of the walls plays an important role in the critical germ: if the steepness of the wall is decreased (increased), the critical radius increases (decreases) and a dipole current can stabilize bubbles with large (small) radius. We emphasize that the bubbles studied in this work are different from the non-topological dark solitons studied in NLS systems with competing interactions.^{53,54} Bubbles are unstable in such NLS systems and competing interactions occur homogeneously in space. On the contrary, bubbles in our sG system are stabilized by a space-dependent external force and competing interactions occur only in a localized region of space due to the heterogeneity of the force.

As a final remark, notice that if we consider large deviations from the bubble solution (2) and the coaxial current (3) and (4), the system will also show large deviations from the original behavior. However, our results will not change substantially if the topological properties of the modified profiles are preserved, according to the qualitative theory of nonlinear dynamical systems.⁴⁷ Thus, any system that resembles ours in the form of the bubble solution (2) or coaxial current (3) and (4) will have the same qualitative behavior near separatrices and fixed points. This point is extensively

addressed in the literature.^{33,34,39,59} In our case, any localized force with a fixed point at a certain value of r surrounded by two extreme values will be qualitatively equivalent to Eq. (3). Similarly, any bubble solution with a kink-like profile connecting the phases $\phi_0 := 0$ and $\phi_1 := 2\pi$ will be qualitatively equivalent to Eq. (2).

We conclude that the dynamics of fluxon bubbles in our system is a robust phenomenon. Indeed, the results presented in this article can be extended to other systems with topologically similar heterogeneities. A particular example is the following superposition of Gaussian-like functions:

$$G(r) = \gamma \left[e^{-\frac{1}{2\sigma^2}(r-r_o+a)^2} - e^{-\frac{1}{2\sigma^2}(r-r_o-a)^2} \right], \tag{14}$$

which is depicted in Fig. 13 for the given values of the parameters. It is asserted that F_+ and G are topologically equivalent forces for the corresponding values of the parameters. For the force F_+ , we have obtained analytical solutions in full agreement with the numerical simulations shown in Fig. 9(a). Notwithstanding this, numerical simulations under the force G show qualitatively the same results. For the following set of parameters $\{\gamma, \sigma, r_o, a\}$: $\{0.9, 0.8, 30.0, 0.4\}$, $\{0.9, 0.8, 29.0, 0.4\}$, force (14) reproduces the same results shown in Figs. 4(b) and 4(d), respectively. It is also possible to reproduce all the phenomena reported in this article using, for instance, the following bubble-like profile:

$$\phi_N(r) = \frac{H}{2} \left[\tanh\left(\frac{r+r_o}{S}\right) + \tanh\left(\frac{r_o-r}{S}\right) \right]. \tag{15}$$

For $H = 2\pi$, ϕ_N and ϕ_+ are topologically equivalent bubbles. For the following set of parameters $\{S, r_o\}$: $\{3.5, 8.7\}$, $\{6.5, 16.0\}$, bubble (15) driven by the force F_+ in Eq. (3) reproduces the same results shown in Figs. 8(b) and 9(a), respectively. The results are robust even in the presence of small-amplitude additive noise in the sG equation (1), whose physical origin can be attributed, for instance, to thermal fluctuations.⁶⁴ In brief, we have reproduced all the results presented in this article using several combinations of the parameters of G and ϕ_N .

In summary, the results of this article provide a robust and general mechanism of control, trapping, and breaking of bubble fluxons in JJ devices. Our analytical results are in good agreement with numerical simulations and suggest a promising way for the storage and transport of heat and information in quantum information devices.

SUPPLEMENTARY MATERIAL

See the [supplementary material](#) video for an overview of the bubble fluxon dynamics in 2 + 1 dimensions using different combinations of parameters.

ACKNOWLEDGMENTS

The authors are grateful to Nicolás Tejos for his advice on the manuscript. M.A.G.-N. acknowledges financial support of the Proyecto Interno Regular PUCV (No. 033.363/2019). J.F.M. acknowledges financial support of the CONICYT-PCHA/Doctorado Nacional (No. 2015-21150292) and the Universidad de Santiago de Chile through the POSTDOC_DICYT (Grant No. 042031GZ_POSTDOC).

DATA AVAILABILITY

The data from numerical simulations that support the findings of this study are available from the corresponding author upon reasonable request.

REFERENCES

- 1 J. Cuevas-Maraver, P. Kevrekidis, and F. Williams, *The Sine-Gordon Model and its Applications* (Springer International Publishing, 2014).
- 2 A. V. Ustinov, T. Doderer, R. P. Huebener, N. F. Pedersen, B. Mayer, and V. A. Obobnov, "Dynamics of sine-Gordon solitons in the annular Josephson junction," *Phys. Rev. Lett.* **69**, 1815–1818 (1992).
- 3 A. Ustinov, "Solitons in Josephson junctions," *Physica D* **123**, 315–329 (1998).
- 4 C. Gorria, Y. B. Gaididei, M. P. Soerensen, P. L. Christiansen, and J. G. Caputo, "Kink propagation and trapping in a two-dimensional curved Josephson junction," *Phys. Rev. B* **69**, 134506 (2004).
- 5 S. Lin and X. Hu, "Possible dynamic states in inductively coupled intrinsic Josephson junctions of layered high- T_c superconductors," *Phys. Rev. Lett.* **100**, 247006 (2008).
- 6 M. G. Clerc, S. Coulibaly, and D. Laroze, "Localized states beyond the asymptotic parametrically driven amplitude equation," *Phys. Rev. E* **77**, 056209 (2008).
- 7 E. Berrios-Caro, M. G. Clerc, and A. O. Leon, "Flaming 2π kinks in parametrically driven systems," *Phys. Rev. E* **94**, 052217 (2016).
- 8 M. Blaauboer, B. A. Malomed, and G. Kurizki, "Spatiotemporally localized multidimensional solitons in self-induced transparency media," *Phys. Rev. Lett.* **84**, 1906–1909 (2000).
- 9 H. Leblond and D. Mihalache, "Few-optical-cycle solitons: Modified Korteweg-de Vries sine-Gordon equation versus other non-slowly-varying-envelope-approximation models," *Phys. Rev. A* **79**, 063835 (2009).
- 10 F. Geniet and J. Leon, "Energy transmission in the forbidden band gap of a nonlinear chain," *Phys. Rev. Lett.* **89**, 134102 (2002).
- 11 O. M. Braun and Y. Kivshar, *The Frenkel-Kontorova Model* (Springer-Verlag, Berlin, 2004).
- 12 K. Alfaro-Bittner, M. G. Clerc, M. A. García-Núñez, and R. G. Rojas, " π -kink propagation in the damped Frenkel-Kontorova model," *Europhys. Lett.* **119**, 40003 (2017).
- 13 A. V. Ustinov, "Fluxon insertion into annular Josephson junctions," *Appl. Phys. Lett.* **80**, 3153–3155 (2002).
- 14 B. A. Malomed and A. V. Ustinov, "Creation of classical and quantum fluxons by a current dipole in a long Josephson junction," *Phys. Rev. B* **69**, 064502 (2004).
- 15 R. Menditto, M. Merker, M. Siegel, D. Koelle, R. Kleiner, and E. Goldobin, "Evidence of macroscopic quantum tunneling from both wells in a φ Josephson junction," *Phys. Rev. B* **98**, 024509 (2018).
- 16 L. G. Aslamazov and E. V. Gurovich, "Pinning of solitons by Abrikosov vortices in distributed Josephson junctions," *JETP Lett.* **40**, 746–749 (1984).
- 17 E. V. Gurovich and V. G. Mikhalev, "Interaction between breathers and fluxon 'bundles' with microshorts, Abrikosov vortices, and local currents in distributed Josephson junctions," *Zh. Eksp. Teor. Fiz.* **93**, 1293–1298 (1987).
- 18 R. Fehrenbacher, V. B. Geshkenbein, and G. Blatter, "Pinning phenomena and critical currents in disordered long Josephson junctions," *Phys. Rev. B* **45**, 5450–5467 (1992).
- 19 D. R. Gulevich and F. V. Kusmartsev, "Flux cloning in Josephson transmission lines," *Phys. Rev. Lett.* **97**, 017004 (2006).
- 20 D. R. Gulevich and F. V. Kusmartsev, "New phenomena in long Josephson junctions," *Supercond. Sci. Technol.* **20**, S60 (2007).
- 21 R. Monaco and J. Mygind, "Fluxon dynamics in elliptic annular Josephson junctions," *J. Low Temp. Phys.* **183**, 1–13 (2016).
- 22 K. O'Brien, C. Macklin, I. Siddiqi, and X. Zhang, "Resonant phase matching of Josephson junction traveling wave parametric amplifiers," *Phys. Rev. Lett.* **113**, 157001 (2014).
- 23 C. Macklin, K. O'Brien, D. Hover, M. E. Schwartz, V. Bolkhovskiy, X. Zhang, W. D. Oliver, and I. Siddiqi, "A near-quantum-limited Josephson traveling-wave parametric amplifier," *Science* **350**, 307–310 (2015).
- 24 T. Fujii, T. Shibata, M. Nishida, and N. Hatakenaka, "Flying superconducting qubits," *IEEE Trans. Appl. Supercond.* **17**, 97–100 (2007).
- 25 D. Kafri, P. Adhikari, and J. M. Taylor, "Dynamics of an ion coupled to a parametric superconducting circuit," *Phys. Rev. A* **93**, 013412 (2016).
- 26 F. Albarrán-Arriagada, L. Lamata, E. Solano, G. Romero, and J. C. Retamal, "Spin-1 models in the ultrastrong-coupling regime of circuit QED," *Phys. Rev. A* **97**, 022306 (2018).
- 27 C. Guarcello, P. Solinas, A. Braggio, and F. Giazotto, "Phase-coherent solitonic Josephson heat oscillator," *Sci. Rep.* **8**, 12287 (2018).
- 28 C. Guarcello, P. Solinas, A. Braggio, and F. Giazotto, "Solitonic thermal transport in a current-biased long Josephson junction," *Phys. Rev. B* **98**, 104501 (2018).
- 29 S.-Y. Hwang, F. Giazotto, and B. Sothmann, "Phase-coherent heat circulator based on multi-terminal Josephson junctions," *Phys. Rev. Appl.* **10**, 044062 (2018).
- 30 C. Guarcello, A. Braggio, P. Solinas, and F. Giazotto, "Nonlinear critical-current thermal response of an asymmetric Josephson tunnel junction," *Phys. Rev. Appl.* **11**, 024002 (2019).
- 31 M. Peyrard and T. Dauxois, *Physique des Solitons* (Savoires actuels, 2004).
- 32 J. A. González, A. Bellorín, and L. E. Guerrero, "Internal modes of sine-Gordon solitons in the presence of spatiotemporal perturbations," *Phys. Rev. E* **65**, 065601(R) (2002).
- 33 J. A. González, A. Bellorín, and L. E. Guerrero, "How to excite the internal modes of sine-Gordon solitons," *Chaos Soliton. Fract.* **17**, 907–919 (2003).
- 34 M. A. García-Núñez, J. F. Marín, and J. A. González, "Bubblelike structures generated by activation of internal shape modes in two-dimensional sine-Gordon line solitons," *Phys. Rev. E* **95**, 032222 (2017).
- 35 J. Geicke, "Cylindrical pulsions in nonlinear relativistic wave equations," *Phys. Scr.* **29**, 431–434 (1984).
- 36 P. L. Christiansen, N. Grønbech-Jensen, P. S. Lomdahl, and B. A. Malomed, "Oscillations of eccentric pulsions," *Phys. Scr.* **55**, 131–134 (1997).
- 37 S. Ahmad, H. Susanto, J. A. D. Wattis, and E. Goldobin, "Existence and stability analysis of semifluxons in disk-shaped two-dimensional $0-\pi$ Josephson junctions," *Phys. Rev. B* **82**, 174504 (2010).
- 38 P. G. Kevrekidis, I. Danaila, J.-G. Caputo, and R. Carretero-González, "Planar and radial kinks in nonlinear Klein-Gordon models: Existence, stability, and dynamics," *Phys. Rev. E* **98**, 052217 (2018).
- 39 J. F. Marín, "Generation of soliton bubbles in a sine-Gordon system with localised inhomogeneities," *J. Phys. Conf. Ser.* **1043**, 012001 (2018).
- 40 J. A. González, A. Bellorín, M. A. García-Núñez, L. Guerrero, S. Jiménez, J. F. Marín, and L. Vázquez, "Fate of the true-vacuum bubbles," *J. Cosmol. Astropart. Phys.* **2018**, 033 (2018).
- 41 M. Kamranian, M. Dehghan, and M. Tatarı, "Study of the two-dimensional sine-Gordon equation arising in Josephson junctions using meshless finite point method," *Int. J. Numer. Model. El.* **30**, e2210 (2017).
- 42 S. Johnson, P. Suarez, and A. Biswas, "New exact solutions for the sine-Gordon equation in 2 + 1 dimensions," *Comput. Math. Math. Phys.* **52**, 98–104 (2012).
- 43 J. T. Giblin, L. Hui, E. A. Lim, and I. S. Yang, "How to run through walls: Dynamics of bubble and soliton collisions," *Phys. Rev. D* **82**, 045019 (2010).
- 44 A. Barone and G. Paternò, *Physics and Applications of the Josephson Effect* (Wiley, 1982).
- 45 B. A. Malomed, "The sine-Gordon model: General background, physical motivations, inverse scattering, and solitons," in *The Sine-Gordon Model and Its Applications, Nonlinear Systems and Complexity Vol. 10*, edited by F. Williams, J. Cuevas-Maraver, and P. Kevrekidis (Springer International Publishing, 2014), Chap. 1.
- 46 B. A. Malomed, "Dynamics of quasi-one-dimensional kinks in the two-dimensional sine-Gordon model," *Physica D* **52**, 157–170 (1991).
- 47 J. Guckenheimer and P. Holmes, *Nonlinear Oscillations, Dynamical Systems, and Bifurcations of Vector Fields* (Springer-Verlag, New York, 1986).
- 48 W. van Saarloos and P. C. Hohenberg, "Pulses and fronts in the complex Ginzburg-Landau equation near a subcritical bifurcation," *Phys. Rev. Lett.* **64**, 749–752 (1990).
- 49 P. L. Christiansen and P. S. Lomdahl, "Numerical study of 2 + 1 dimensional sine-Gordon solitons," *Physica D* **2**, 482–494 (1981).
- 50 J. González, A. Marciano, B. Mello, and L. Trujillo, "Controlled transport of solitons and bubbles using external perturbations," *Chaos Soliton. Fract.* **28**, 804–821 (2006).

- ⁵¹P. Christiansen and O. Olsen, "Return effect for rotationally symmetric solitary wave solutions to the sine-Gordon equation," *Phys. Lett. A* **68**, 185–188 (1978).
- ⁵²P. L. Christiansen and O. H. Olsen, "Ring-shaped quasi-soliton solutions to the two- and three-dimensional sine-Gordon equation," *Phys. Scr.* **20**, 531–538 (1979).
- ⁵³I. Barashenkov, A. Gocheva, V. Makhankov, and I. Puzynin, "Stability of the soliton-like "bubbles"," *Physica D* **34**, 240–254 (1989).
- ⁵⁴I. V. Barashenkov and E. Y. Panova, "Stability and evolution of the quiescent and travelling solitonic bubbles," *Physica D* **69**, 114–134 (1993).
- ⁵⁵J. A. González and J. A. Holyst, "Behavior of ϕ^4 kinks in the presence of external forces," *Phys. Rev. B* **45**, 10338–10343 (1992).
- ⁵⁶S. Flügge, *Practical Quantum Mechanics* (Springer Science & Business Media, 2012).
- ⁵⁷J. A. Holyst and H. Benner, "Universal family of kink-bearing models reconstructed from a Pöschl–Teller scattering potential," *Phys. Rev. B* **43**, 11190–11196 (1991).
- ⁵⁸M. Peyrard and D. K. Campbell, "Kink–antikink interactions in a modified sine-Gordon model," *Physica D* **9**, 33–51 (1983).
- ⁵⁹J. A. González, S. Cuenda, and A. Sánchez, "Kink dynamics in spatially inhomogeneous media: The role of internal modes," *Phys. Rev. E* **75**, 036611 (2007).
- ⁶⁰J. A. González and F. A. Oliveira, "Nucleation theory, the escaping processes, and nonlinear stability," *Phys. Rev. B* **59**, 6100–6105 (1999).
- ⁶¹A. Filippov, Y. Kuzovlev, and T. Soboleva, "On the structure of critical nuclei at first-order phase transitions in 3D systems," *Phys. Lett. A* **165**, 159–164 (1992).
- ⁶²V. I. Khvorostyanov and J. A. Curry, "Thermodynamic theory of freezing and melting of water and aqueous solutions," *J. Phys. Chem. A* **108**, 11073–11085 (2004).
- ⁶³B. Scheifele, I. Saika-Voivod, R. K. Bowles, and P. H. Poole, "Heterogeneous nucleation in the low-barrier regime," *Phys. Rev. E* **87**, 042407 (2013).
- ⁶⁴J. Mazo and A. V. Ustinov, "The sine-Gordon equation in Josephson-junction arrays," in *The Sine-Gordon Model and Its Applications: From Pendula and Josephson Junctions to Gravity and High-Energy Physics*, edited by J. Cuevas-Maraver, P. G. Kevrekidis, and F. Williams (Springer International Publishing, Cham, 2014), pp. 155–175.